Supplement

Ioannis Katharopoulos

October 20, 2022

S-1 Figures

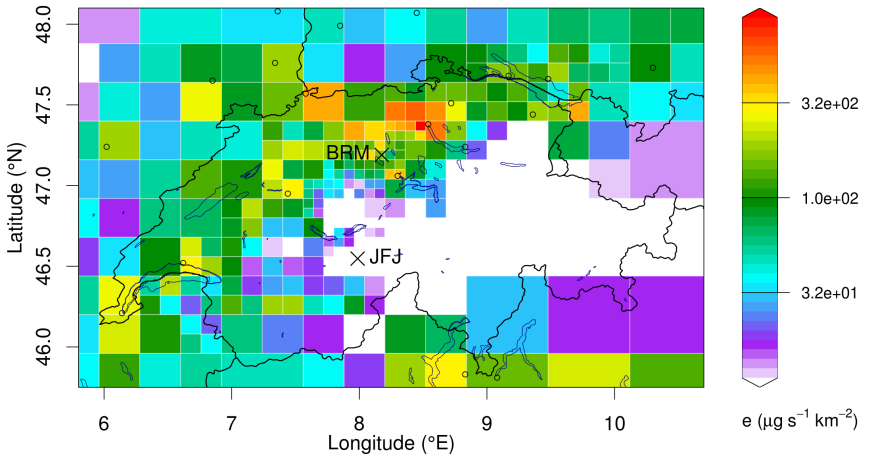

Figure S1: Spatial distribution of Swiss HFC-125 a-posteriori emissions for the base inversion (BRM and JFJ only included) for the period 2019–2020 with the 7 km model starting from a population based a-priori.

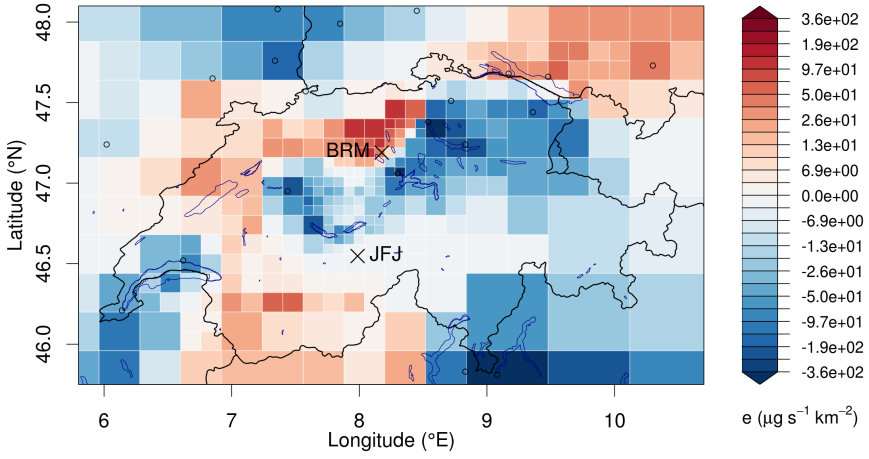

Figure S2: A-posteriori minus a-priori emission differences for HFC-125 for the base inversion with the 7 km model starting from a population based a-priori.

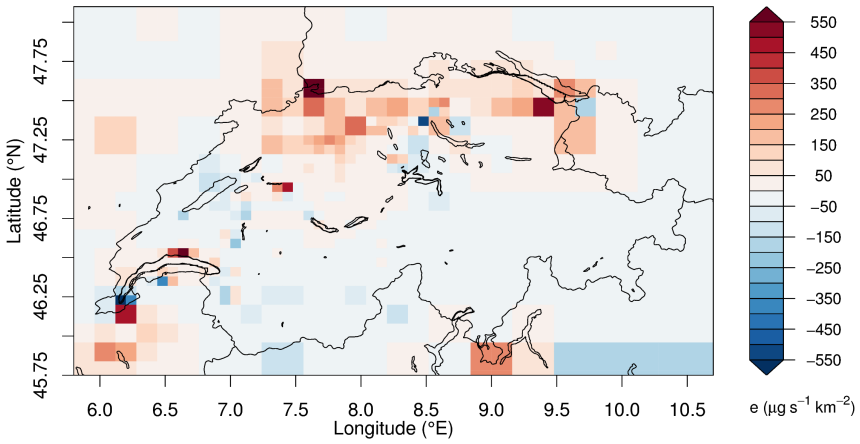

Figure S3: A-posteriori emission differences between the high- and low-resolution model inversions with population based a-priori for HFC-125

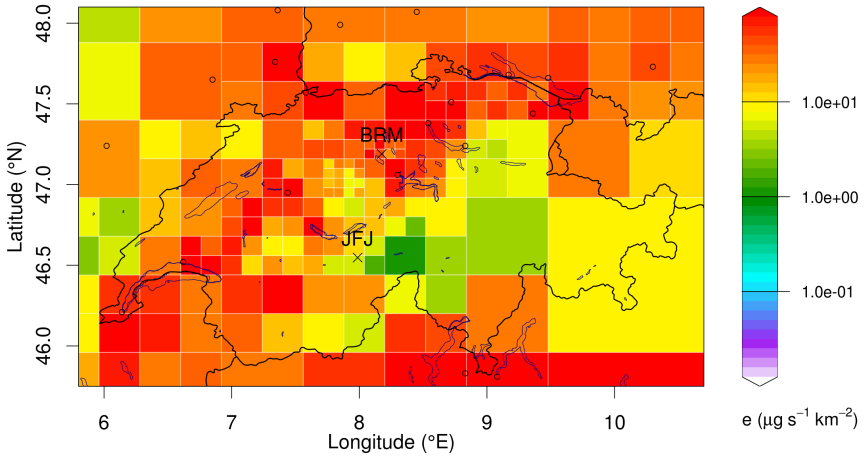

Figure S4: Spatial distribution of Swiss HFC-32 a-posteriori emissions for the base inversion (BRM and JFJ only included) for the period 2019–2020 with the 7 km model starting from a population based a-priori.

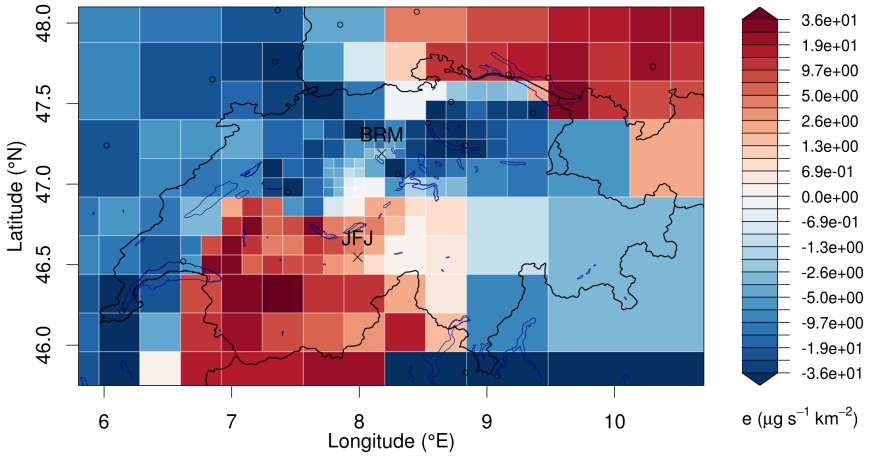

Figure S5: A-posteriori minus a-priori emission differences for HFC-125 for the base inversion with the 7 km model starting from a population based a-priori.

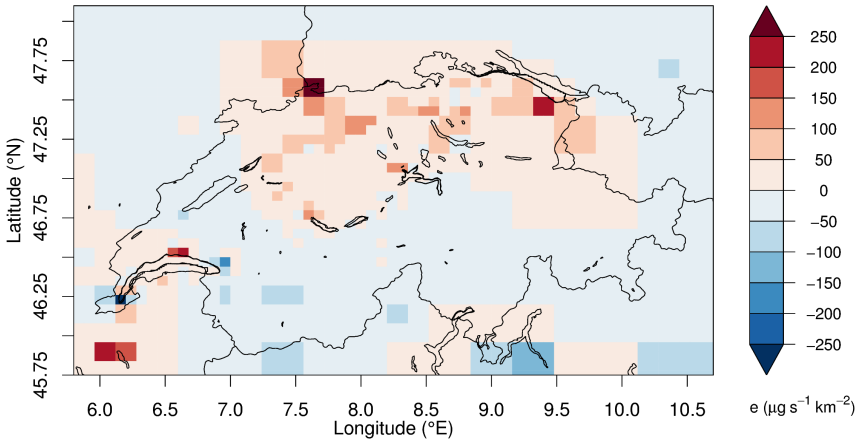

Figure S6: A-posteriori emission differences between the high- and low-resolution model inversions with population based a-priori for HFC-125

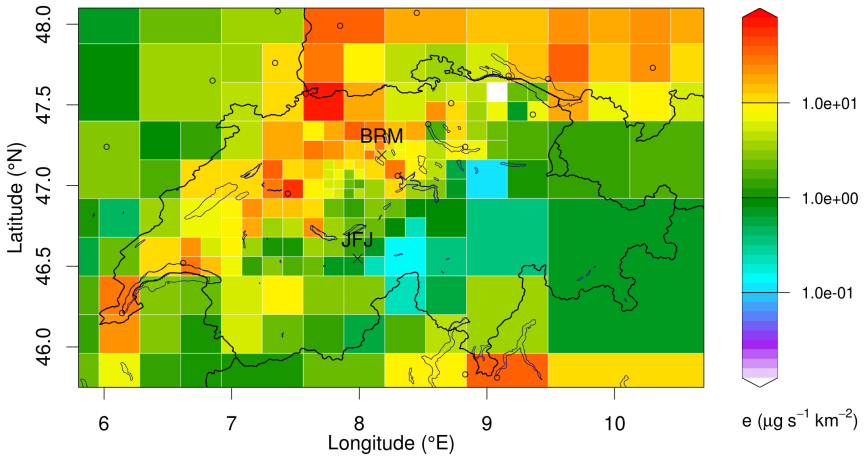

Figure S7: Spatial distribution of Swiss HFC-125 a-posteriori emissions for the base inversion (BRM and JFJ only included) for the period 2019–2020 with the 7 km model starting from a population based a-priori.

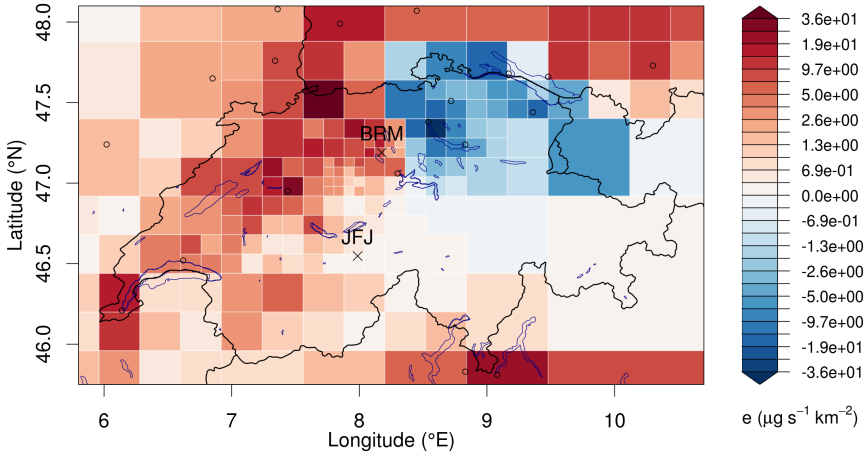

Figure S8: A-posteriori minus a-priori emission differences for HFC-125 for the base inversion with the 7 km model starting from a population based a-priori.

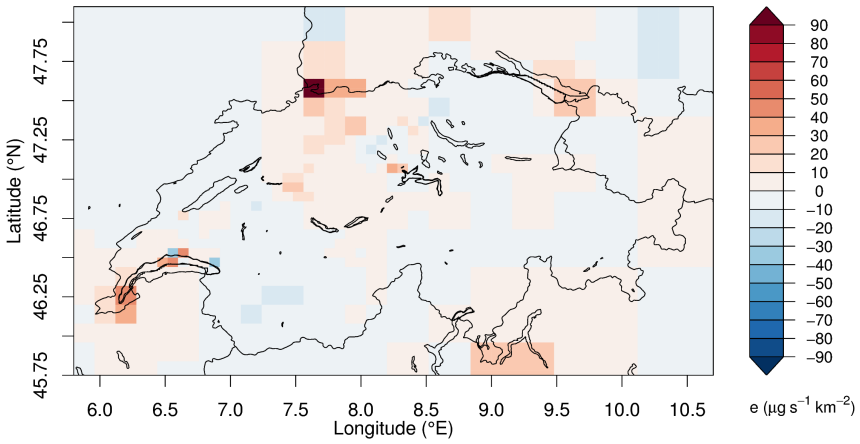

Figure S9: A-posteriori emission differences between the high- and low-resolution model inversions with population based a-priori for HFC-125

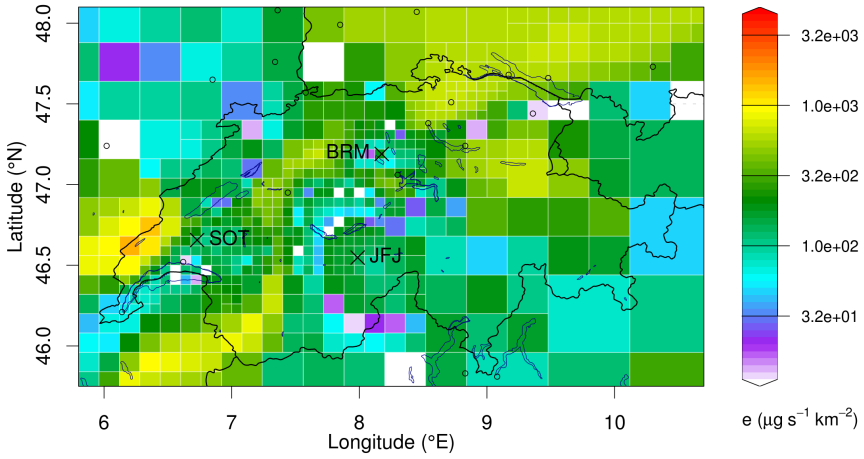

Figure S10: Spatial distribution of Swiss HFC-134a a-posteriori emissions for the inversion including both BRM and SOTT for the period 2019–2021 with the 7 km model starting from a uniform a-priori.

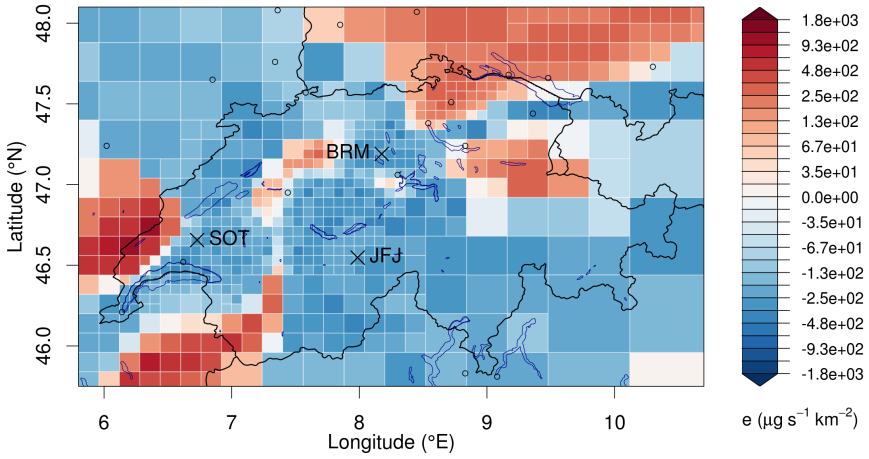

Figure S11: A-posteriori minus a-priori emission differences for HFC-134a for the inversion including both BRM and SOTT for the period 2019–2021 with the 7 km model starting from a uniform a-priori.

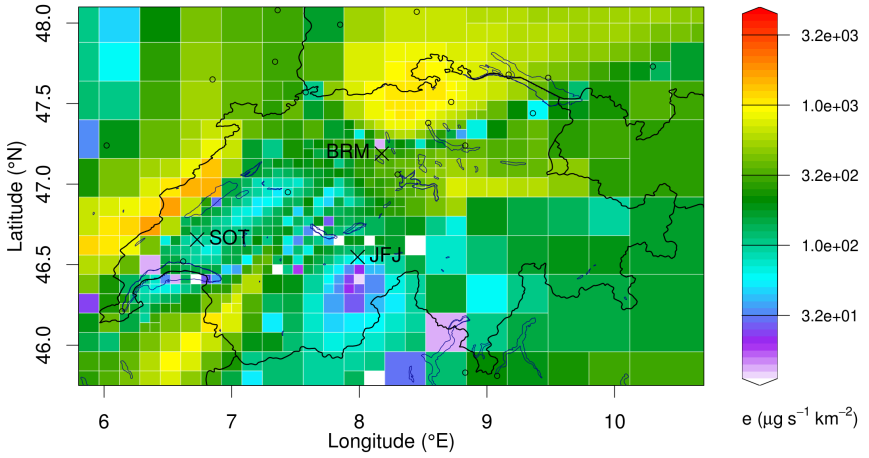

Figure S12: Spatial distribution of Swiss HFC-134a a-posteriori emissions for the inversion including both BRM and SOTT for the period 2019–2021 with the 1 km model starting from a uniform a-priori.

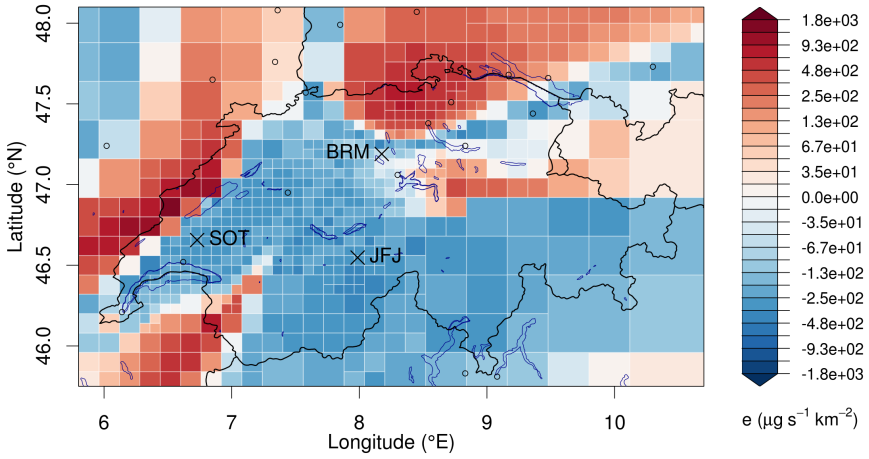

Figure S13: A-posteriori minus a-priori emission differences for HFC-134a for the inversion including both BRM and SOTT for the period 2019–2021 with the 1 km model starting from a uniform a-priori.

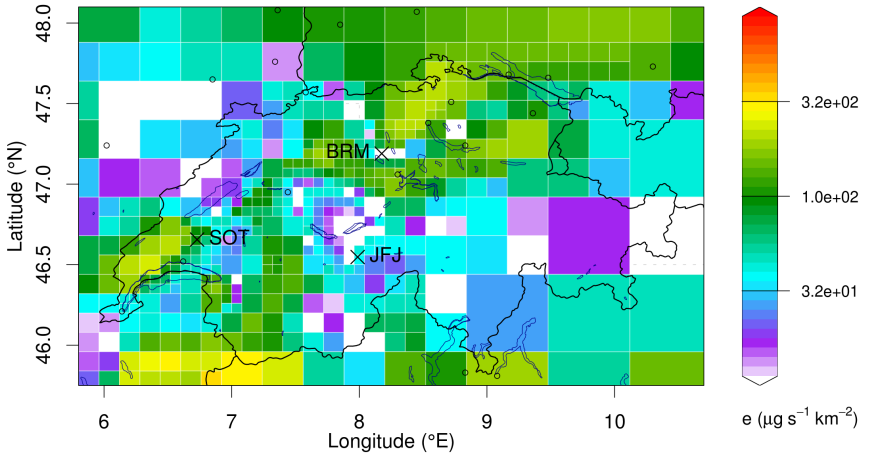

Figure S14: Spatial distribution of Swiss HFC-125 a-posteriori emissions for the inversion including both BRM and SOTT for the period 2019–2021 with the 7 km model starting from a uniform a-priori.

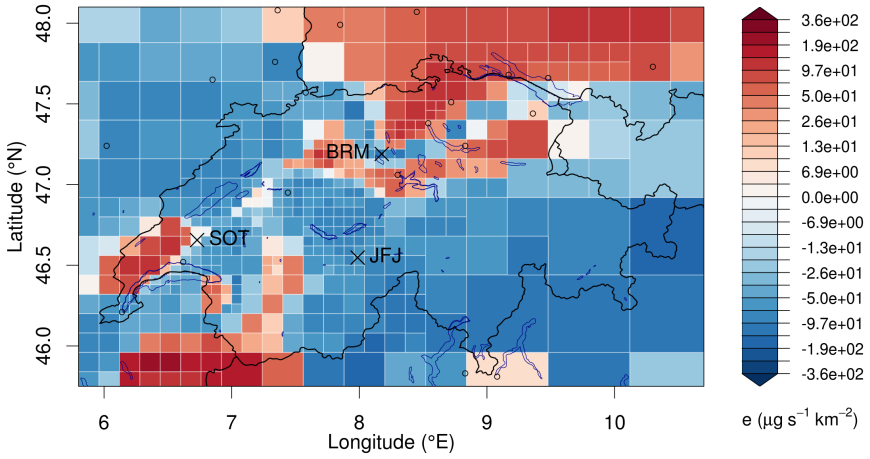

Figure S15: A-posteriori minus a-priori emission differences for HFC-125 for the inversion including both BRM and SOTT for the period 2019–2021 with the 7 km model starting from a uniform a-priori.

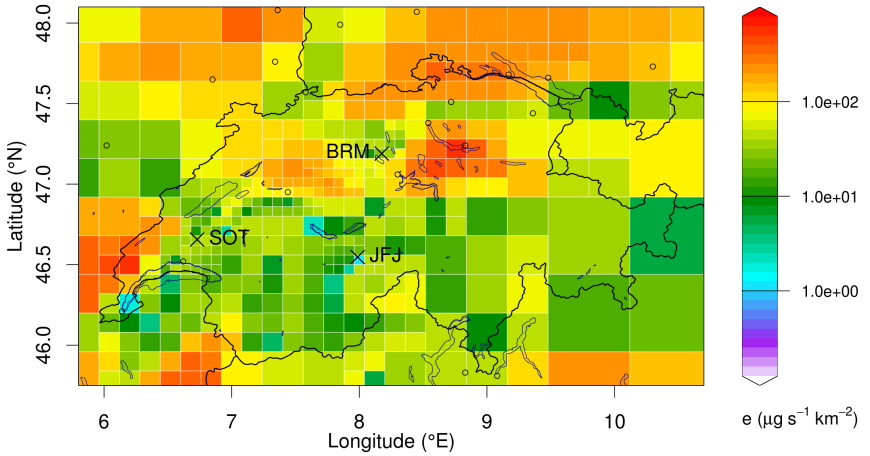

Figure S16: Spatial distribution of Swiss HFC-125 a-posteriori emissions for the inversion including both BRM and SOTT for the period 2019–2021 with the 1 km model starting from a uniform a-priori.

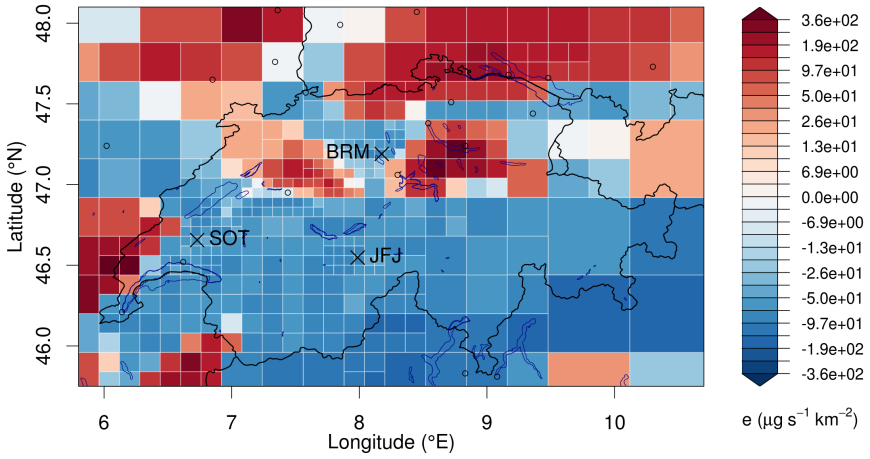

Figure S17: A-posteriori minus a-priori emission differences for HFC-125 for the inversion including both BRM and SOTT for the period 2019–2021 with the 1 km model starting from a uniform a-priori.

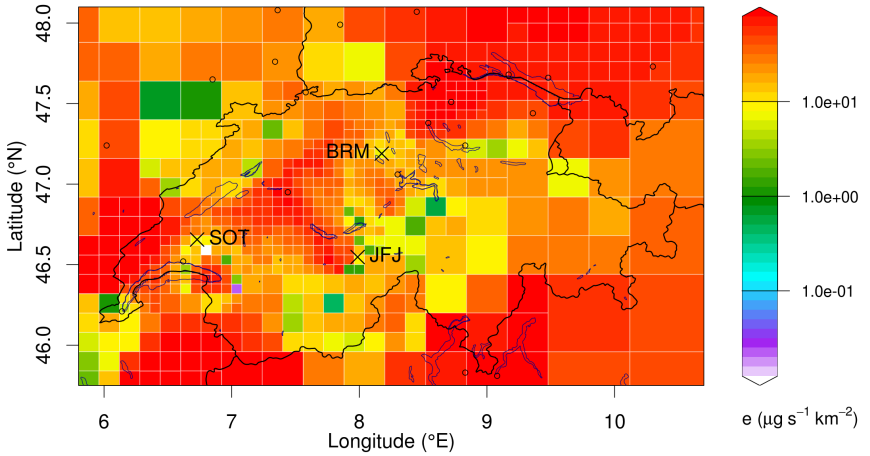

Figure S18: Spatial distribution of Swiss HFC-32 a-posteriori emissions for the inversion including both BRM and SOTT for the period 2019–2021 with the 7 km model starting from a uniform a-priori.

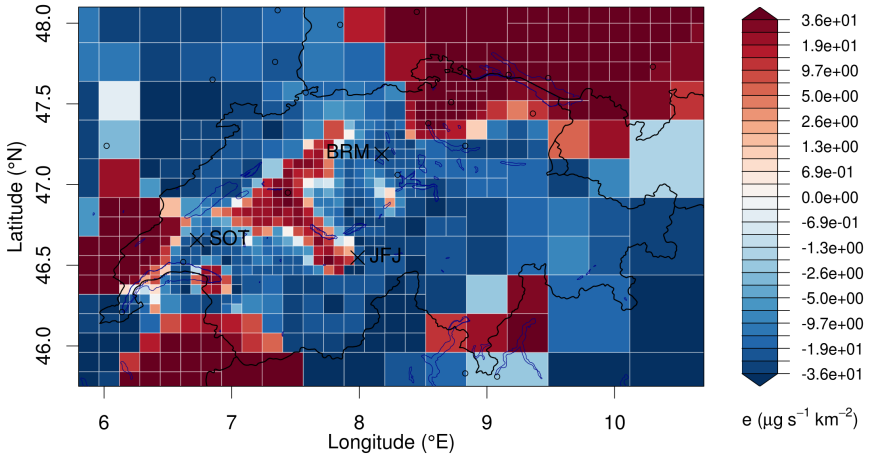

Figure S19: A-posteriori minus a-priori emission differences for HFC-32 for the inversion including both BRM and SOTT for the period 2019–2021 with the 7 km model starting from a uniform a-priori.

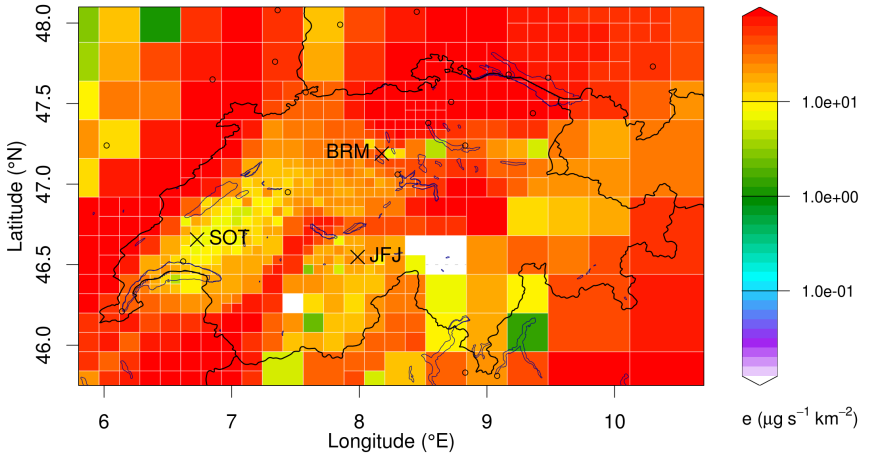

Figure S20: Spatial distribution of Swiss HFC-32 a-posteriori emissions for the inversion including both BRM and SOTT for the period 2019–2021 with the 1 km model starting from a uniform a-priori.

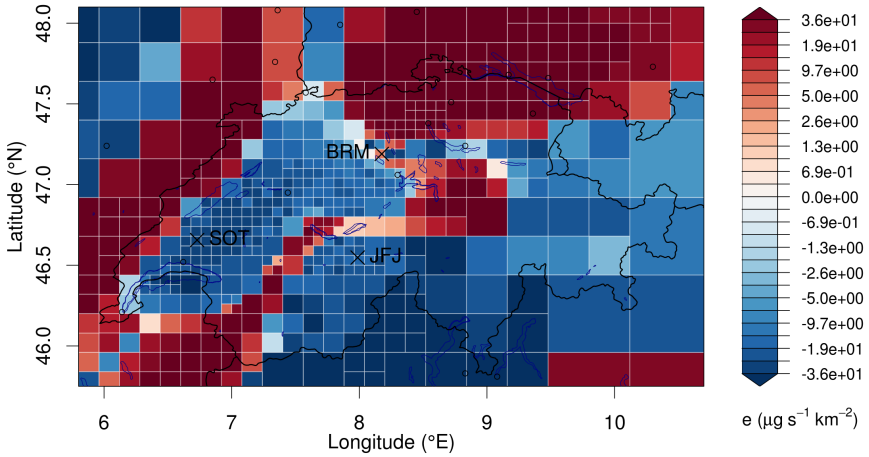

Figure S21: A-posteriori minus a-priori emission differences for HFC-32 for the inversion including both BRM and SOTT for the period 2019–2021 with the 1 km model starting from a uniform a-priori.

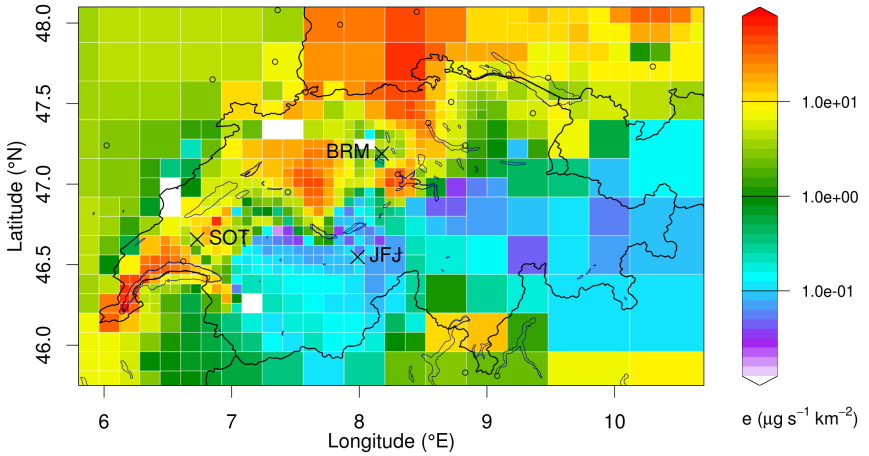

Figure S22: Spatial distribution of Swiss SF_6 a-posteriori emissions for the inversion including both BRM and SOTT for the period 2019–2021 with the 7 km model starting from a uniform a-priori.

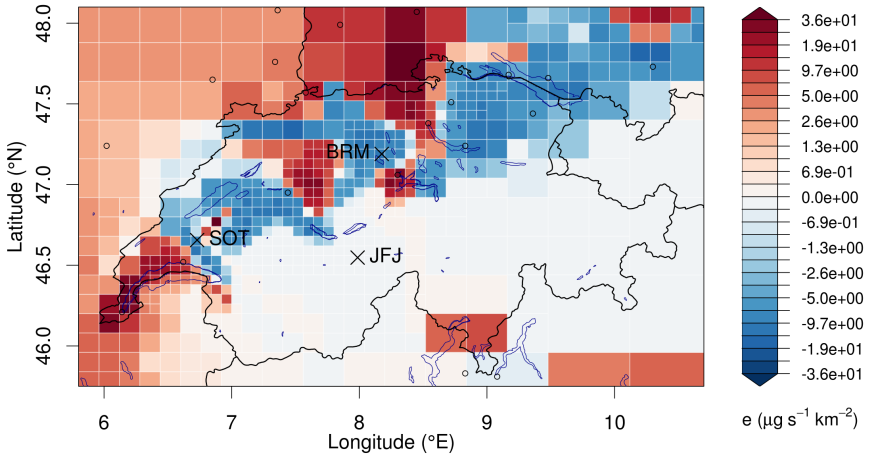

Figure S23: A-posteriori minus a-priori emission differences for SF_6 for the inversion including both BRM and SOTT for the period 2019–2021 with the 7 km model starting from a uniform a-priori.

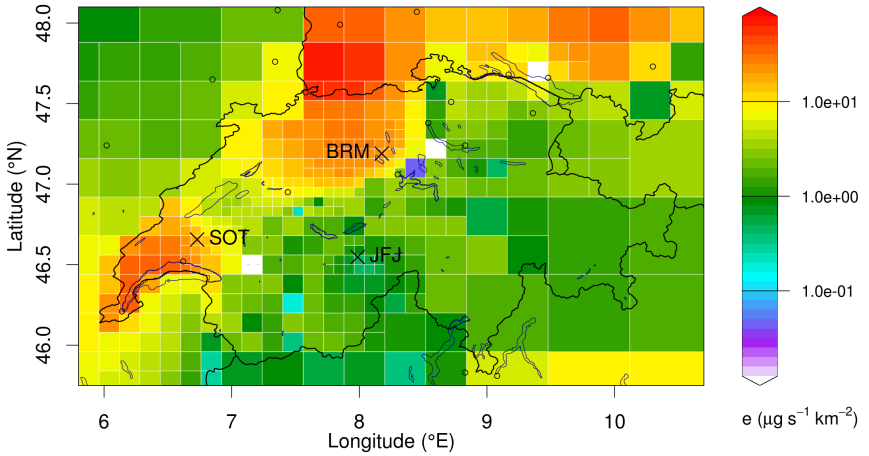

Figure S24: Spatial distribution of Swiss SF_6 a-posteriori emissions for the inversion including both BRM and SOTT for the period 2019–2021 with the 1 km model starting from a uniform a-priori.

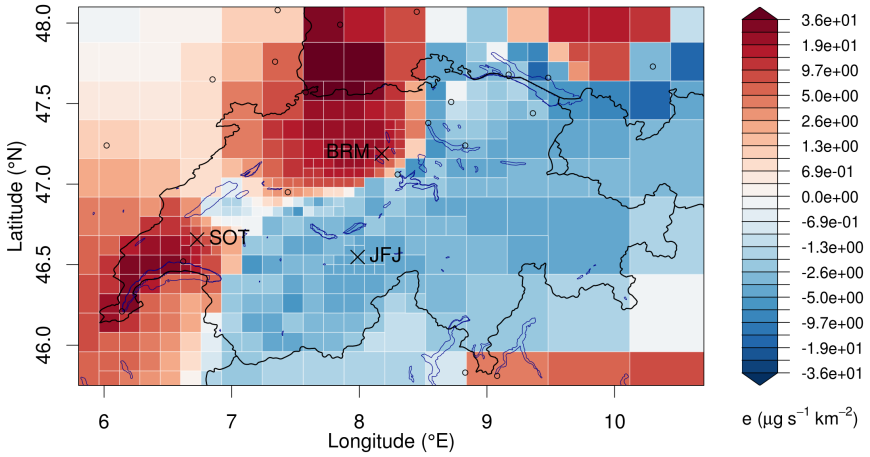

Figure S25: A-posteriori minus a-priori emission differences for SF_6 for the inversion including both BRM and SOTT for the period 2019–2021 with the 1 km model starting from a uniform a-priori.

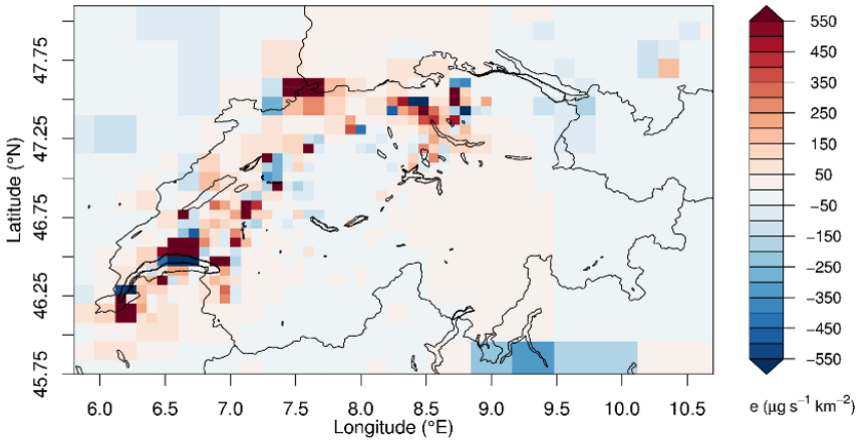

Figure S26: A-posteriori emission differences between the high- model inversions with and without SOTT for a population based a-priori for HFC-134a.